Hydrological and tectonic strain forces measured in a karstic cave using extensometers

Ping ZHU*[1], Michel van Ruymbeke†[1], Yves Quinif[2], Thierry Camelbeeck[1] and Philippe Meus[3]

[1]Royal Observatory of Belgium, ORB-AVENUE CIRCULAIRE 3, 1180, Bruxelles, Belgium.
[2]Institut Jules Cornet (Géologie),Faculté Polytechnique de Mons, Rue de Houdain 9, 7000 Mons,Belgium
[3]Service Public de Wallonie Direction générale opérationnelle Agriculture, Ressources naturelles et Environnement Département de l'Environnement et de l'Eau Direction des Eaux souterraines 15 Avenue Prince de Liege, B-5100 Jambes, Belgium

*ping.zhu@observatoire.be
†labvruy@oma.be

In order to monitor the hydrological strain forces of the karst micro fissure networks and local fault activities, six capacitive extensometers were installed inside a karstic cave near the midi-fault in Belgium. From 2004 to 2008, the nearby Lomme River experienced several heavy rains, leading to flooding inside the Rochefort cave. The highest water level rose more than thirteen meters, the karstic fissure networks were filled with water, which altered the pore pressure of the cave. The strain response to the hydrological induced pore pressure changes are separately deduced from fifteen events when the water level exceeded six meters. The strain measured from the extensometer show a linear contraction during the water recharge and a nonlinear exponential extension releasing during the water discharge. The sensitivity and stability of the sensor are constrained by comparing continuously observed tidal strain waves with a theoretical model. Finally, a local fault deformation rate around 0.03 ± 0.002mm/yr is estimated from more than four years' records.

Keywords: Hydrologic, Tectonic, Tides, Strain, Deformation

1 INTRODUCTION

The Rochefort karstic cave is located at a relatively stable continental region where the seismicity and the risk of seismic hazard are low. Palaeoseismology studies indicate that a maximum 0.3mm/yr deformation rate could account for coseismic effects from three large earthquakes during the Pleistocene and Holocene (Camelbeeck and Meghraoui, 1998). However, the recently growing stalagmite and falling rocks inside the cave, strongly evidence that the identified faults are active and expending in the NW-SE direction, driven by the regional tectonic force (Vandycke and Quinif, 2001). But the continuous GPS measurements show motions less than 1mm/yr which is still inside the error bar. Hence, to constrain the results provided by the geological investigations, an in-situ strain measurement experiment was conducted since 1999.

Beyond its interest about the local faults activities, the experiment is also focusing on providing information about the hydrological impact on the formations process of micro fissure networks and karstification. There are two kinds of water flux which contribute to the process, the slow seepage and fast flow drainage. To monitor the strain inside a cave can help improving the understanding of the karst structure, especially it's porosity and fissure networks (Genty and Deflandre, 1998).

Six extensometers were set up near two identified faults inside the Rochefort cave, two aluminum extensometers No.1 (E1) and No.2 (E2) in 1997 and four Pyrex aluminum extensometers No.3 (E3), No.4 (E4), No.5 (E5), and No.6 (E6) in 2000. The hydrological strain forces, local faults activity, and the secular earth strain were detected from the recording of the extensometers.

2 EXPERIMENT SITE

The Rochefort karstic caves are located 20km away from the midi-fault, along which an Ms4.6 earthquake occurred on Aug. 08, 1988. At the far north-east direction, this area is a relatively active zone: all of the 'Roer Valley' graben is bounded by two normal faults, the Peel Fault (PF) and the Feldbiss Fault (FF). An Ms 5.3 earthquake occurred on Apr. 13, 1992 along the PF (Camelbeeck and Meghraoui, 1996).In this region, the majority of earthquakes were located at both sides of the midi-fault according to the Earthquake Catalog of Royal Observatory of Belgium (ROB) since 1910 (Fig.1). The Rochefort cave is buried 50 meters underground and constituted by two galleries: large one along the stratigraphic direction (N070E) named 'Fontaine Bagdad' and smaller one in the dip direction 'Val d'Enfer'. Inside the cave, two types of faults are recognized (Fig.1). The first type of fault is contemporaneous of the Variscan folding, characterized by reverse motion along the bedding planes. The second type is the present active faults. The recent faults are related with present-day tectonic activity which is evidenced by seismicity of the neighbor area. The stereographic projection of recent faults affecting Rochefort karstic network shows a principal NW-SE extension, nearly perpendicular to the present regional stress as illustrated by the analysis of the last strong regional earthquake (Vandycke and

Quinif, 2001).

Three water table probes have been successively installed inside the Rochefort karstic caves since 2005 (Fig.1). The first one (WI) was set up under the 'Val d'Enfer' room on March 2005. The site was at the bottom of an irregular shaft, about 77 meters deep and a few meters in section. The second one (WII) was installed at the 'Rivière des Touristes' in 2006. The 'Rivière des Touristes' is at one of the deepest points inside the cave. It is behaving as a river; the water comes from a sump and then flow out into another sump. During the flood period, the nearby conduits were filled and then the river becomes a lake. The third one (WIII) was placed at the 'Petit Noir' on 2007, located at a large funnel shape hall which is the ultimate point of the cave.

3 EXTENSOMETER

The Pyrex aluminum capacitive extensometers were designed and developed in 1999 at the Royal Observatory of Belgium in Brussels. The gauge is consisted of two round aluminum plates with 40mm diameter and it is fixed in the rock by two Pyrex rods. The extensometers were installed in two steps: first, two fiducial points are drilled 6cm into the limestone at two sides of a fault then the Pyrex rods are bonded to the hole by a chemical anchor capsules (Upat-UKA3); Second, about one month later, when the piers are adequately bounded with the rocks, we mount the extensometers with a 1300°C flame. The dielectricity of the capacitance is directly counted by an electric oscillator chip. EDAS data logger was used as acquisition systems (Van Ruymbeke et al., 2001; Sondag et al., 2003). The initial sampling interval is one minute. The laboratory calibration experiments show that the counting frequency is linearly proportional to the displacement when the relative displacement is less than 100μm. The stability and sensitivity of the gauges are influenced by the humidity, pressure, and temperature since the sensors are completely exposed to the environment. Fortunately, the meteorological conditions are very stable inside the cave. The continuous rock temperature monitoring near E4 gave an annual temperature variations of about 0.06°C, and the maximum daily changes were less than 0.02°C. The thermal expansion coefficient is 22.3×10^{-6} for aluminum and 3.25×10^{-6} for Pyrex glass. Thus, taking into account the laboratory tests, the expected strain resolution should be better than 0.1ppm. The original data were decimated into hour sampling rate (Fig.2). We selected the most homogeneous records of E4 (length 81mm, azimuth $84°$), E5 (length 92mm, azimuth $136°$) and E6 (length 75mm, azimuth $58°$) since 2003, three years after the installation. Therefore we can believe that the extensometers are adequately coupled with the host rocks.

4 RESULTS

4.1 TIDAL STRAIN

The most difficult problem for such experiment is the calibration and evaluation of the stability of the sensors. The solid Earth Tides, continuously registered on the E4, E5 and E6, provide us a stable reference. The tidal strain measurement began from 1951 when Sassa, Ozawa and Yoshikawa published the first results obtained with a superinvar wire extensometer (Melchior, 1983). After that, a great effort have been paid to design high accuracy strainmeters by different groups, among them the most reliable gauges should be the Laser strain meter (Berger and Lovberg, 1970; King and Bilham, 1973; Berger and Wyatt, 1973; Sydenham, 1974; Beavan and Goulty, 1977). With the new technology, the secular earth strain tides can be easily observed in different places. Thus, the interests of strain observations have been moved from the earth tide to seismic toroidal modes, tectonic activities, hydrological effects and transient pre-, co-, or post- seismic signals (Zadro and Braitenberg, 1999).

Due to the high accuracy of the tidal model, the tides are valuable input signals for the instruments. It can be applied to calibrate and check the sensitivity of any arbitrary records in situ such as the borehole strain measurements (Westerhaus and Zürn, 2001). The diurnal and semi-diurnal components have been found in the in situ relative seismic velocity variation records in Japan (Yamamura et al., 2003). It allows to measure directly the relation of relative seismic velocity variation with strain. The minimum resolution of our capacitive extensometer can reach 10^{-7}. The synthetic volumetric earth strain tides computed with HW95 tidal potential (Wenzel, 1996) gave the amplitudes are between 10^{-8} and 10^{-9} at the surface of Rochefort karstic caves. Thus the gauges can hardly record the tidal strain by principle. But it is undoubtedly registered at the extensometer 4 and 5. To check the tidal frequency band signals, the data were band pass filtered between 0.6 cycles per day and 8 cycles per day. Two month's results between April, 1st and May 31st in 2005 were plotted (Fig.3 upper). The Amplitude Fourier Spectrum shows the diurnal and semidiurnal solar principal waves and its harmonic components until the fourth (Fig.3 lower). On the E4 these signals are dominated by a stronger one, probably due to the thermal elastic deformation. Similar phenomenon has been reported from a long base line laser strain meter measurements (Berger and Wyatt, 1973). The principal lunar diurnal wave O1 and semidiurnal wave M2 are permanently registered in the gauges E5 with unexpected high signal-to-noise ratio. The theoretical values of the volumetric strain in the azimuth of E5 are computed using Eterna3.3 (Wenzel, 1996) from Apr.01, 2005 to Sep.30, 2005. We compared the phases of O1, M2 and S2 with the records of E5 (Fig.4). The observed phases (O1, M2 and S2) were close to the values of the hydrostatic tidal strain (Table 1). It evidences that the sensors are recording the hydrostatic strains induced by pore pressure changes but the amplitudes were two orders larger than the synthetic values.

4.2 HYDROLOGICAL EFFECTS

The experiment site suffered a relatively dry season from the Feb, 2005 to the beginning of 2006, and then the precipitations were increased. It becomes a rainy season from the mid of 2007 to the end of 2008 (Fig.5 left). When the Lomme River was flooded, the water level rose and fell simultaneously at WI, WII and WIII. Due to the different capacities of three aquifers, they are discharging water with slightly different speeds (Fig.5 right). The WI water level gauge is the nearest probe to the extensometers so that the hydrological induced strain was directly measured on E5 and E6 from WI. To measure the strain changes from the extensometers, a hydrological event is defined when the water level becomes higher than 6 meters. We choice such a definition because the hydrological strain forces signal was superposed on a long term slip trends of fault motion. Sixteen events were located from the records of the water probe since 2005 until 2008. Due to the failure of the power supply, the E5 and E6 have missed one event. The E5 and E6 are well correlated with the processing of water charging and discharging at WI site (Fig.6). Obviously, the response of the extensometers to the charging and discharging procedure were different. The pore pressure was increased when the water level rose and decreased with water discharge.

The fifteen isolated hydrological events were divided into three categories according to the duration of the highest water level. In type one, the process of water charging and discharging is shorter than forty hours. The second type is longer than forty hours, and in the third type, the height of water table is exceeding 6 meters several times in a 150 hours window (Table 2). The highest water level was set as the boundary point between the water charging and discharging. We separately measured the strain changes as a function of water level. Six events were fall into the first category, seven events belong to the second category and two to the last category. During the water charging, the strain rate was linearly proportional to the water level and flux.

At the stage of the water discharge, the strain rate express an exponential recovery to the water level (Fig.7a). It evidently follows this pattern for all events of the second type (Fig.7b). The eighth and fifteenth events belong to the third type, the karst fissure networks were charging and discharging more than one times in a 150 hours window. Both extensometers were instantaneously responding to about one meter water level rising and falling (Fig.7c).

The extensometers simultaneously react to the pore pressure changes which suggest that the pore pressure was altered mainly due to the karst fissure networks were rapidly filling and run-off during the rainy season. In the regional scale, it shows that the complete karstic caves work as an elasticity and homogeneousness media in a short term.

4.3 THE FAULT ACTIVITIES INSIDE THE KARSTIC CAVE

From the beginning of 2005 to the February of 2006, it was a relatively dry season. The water content was decreased inside the cave which altered hydrostatic strain inside the cave. The abnormal contraction appearing on the E6 can be explained by such effects (Fig.2). In 2006, the E5 and E6 were interrupted by a failure of the power supply. The E6

restarted to work after the power supply was repaired. The records of E4, E5, and E6 are decimated into daily sampling rate and low pass filtered to only keep the long term trends with frequency lower than one cycle per month (Fig.8). The annual rock temperature change is 0.06 near the E4. The annual thermal induced elastic deformation deduced from the E4 reaches an amplitude of $7.3 \pm 1.9\mu$m. The thermal effect is obviously weaker at the site of extensometer 5 and 6 where the water are penetrating through the karstic fissure networks and some new stalactites are growing nearby. Each of these three long term trenches was separately fitted by a linear function with 95% confidential boundary. The E4 shows a deformation rate of 0.028mm/yr and 0.026mm/yr for E6. The E6 is bonding across the fault 1 and E4 is to the fault2. It is reasonable to find that the E5 shows a slower expanding rate 0.010mm/yr than the E4 and E6 because the E5 is not directly attached to the identified active faults. The extension direction of the fissure where E5 installed, are nearly perpendicular to the fault 1 and 2.

5 Discussion and conclusions

Diurnal and semidiurnal tidal constituents are continuously recorded by the E5. However, the amplitudes are much greater than the synthetic earth strain tides. But the observed tendency of O1 amplitudes distribution agree well with theoretical value which provides valuable constrains about the stability of the gauge. The solar principal wave S2 and its harmonic components are permanently recorded by the E4 and sometimes the E6. The semidiurnal S2 wave induced by thermal-elastic oscillation with amplitude around 2.4×10^{-7} is clearly observable on the E4. By inter comparing the S2 waves among three sensors, the S2 amplitudes differences were less than 10^{-7}, which confirmed the sensor's stability can reach 0.1ppm (Fig. 4). The amplitudes of observed tidal strain waves are much greater than the theoretical value. It could be attributed to the cavity effects, but due to the chaos of the fractal cavities, it is difficult to model such effects.

Rock deformations induced by hydrological agents were observed from the E5 and E6. The water conductivity and porosity altered the pore pressure inside the cave. These hydrological induced deformations have been found in other geodetic observations. Several solutions are proposed to correct it from the geodetic observations, among them the mostly used methods are the rain function (Langbein et al., 1990) and the predictive filtering methods (Braitenberg, 1999). The E5 and E6 have different maximum strain response to water level. But the rate of strain accumulation and release accompanied by the processing of water charging and discharging, gave coherent results by both gauges for all fifteen events. During the water charging, it shows a linear contraction at E5 and E6 induced by the buoyancy force, at the period of the water discharge. The strain is recovering with an exponential trend due to the pore pressure alternation by the conductivity and porosity of the media during the flood periods. The contraction rate induced by the water level rising is slightly faster for E5 than than E6. After the water release, E5 and E6 share a similar extension rate.

The absolute gravity measurement at the site, shows gravity value increases 90nm/s^2

when the water level rose more than 10 meters (Van Camp et al., 2006). The gravity changes calculated from a 10 meters thick cylinder model in 60 meters depth and with 5% porosity, is 250nm/s^2 Dr. M.Van Camp (pers. comm.). The observed gravity changes are about $1/3$ of the modeled value. Since the strain were linearly reacting to water charging, it suggested that both the strain and gravity changes, can be attributed to the buoyancy force during the water filling the karst fissure networks.

The E6 showed a 0.026mm/yr displacement of fault 1 and E4 gave a 0.028mm/yr displacement of fault2 which was superposed with a $7.3 \pm 1.9\mu$m annual oscillation term. A perpendicular fissure to the fault 1 measured by the E5, gave a 0.010mm/yr rate. The fissure is 20cm in width so that the formation of this fissure is about $20,000$ years if we suppose that the activity of the region is relative stable since it. The expending rate deduced from the E4 and E6, agreed with the results obtained by stereographic projection (Vandycke and Quinif, 2001). It suggests that a local background driving displacement rate is about 0.03 ± 0.002mm/yr. A discussion and a tectonic interpretation of these observations can be found in (Camelbeeck et al., 2012).

A factual karstic cave is normally thought as an unfavorable site for the instrumental observations due to its complex geometry with strong heterogeneity and high humidity rates. But water drips monitoring under the stalactites, raised broad interest for the karstification process and palaeoclimatology study (Genty, 2008). The preliminary results of our strain measurement shed new light on the geophysical experiments. The result suggest that, if the sensor is properly installed, maximum following the characteristics of the nature, the ability of detecting very weak signals like the hydrology, local fault activities and secular earth strain can be achieved.

ACKNOWLEDGMENTS

We are very grateful to the support of Dr. Ronald Van der Linden, director general of Royal Observatory of Belgium. We benefit a lot from the discussions with Dr. Michel Van Camp. We used the ROB earthquake catalog. The first author is financially supported by the Action 2 contract from the Belgian Ministry of Scientific Politics.b The experiments in Rochefort were supported by the Ministry of the Walloon Region(Belgium).

REFERENCES

Beavan, R., Goulty, N., 1977. Earth-strain observations made with the Cambridge laser strainmeter. Geophys.J.R.Astr.Soc. 48, 293–305.

Berger, J., Lovberg, R., 1970. Earth strain measurements with a laser interferometer. Science 170, 296–303.

Berger, J., Wyatt, F., 1973. Some observations of Earth strain tides in California. Phil.Trans.R.Soc.Lond.A. 274, 267–277.

Braitenberg, C., 1999. Estimating the hydrologic induced signal in geodetic measurements with predictive filtering methods. Geophys.Res.Lett. 26, 775–778.

Camelbeeck, T., Meghraoui, M., 1996. Large earthquakes in northern Europe more likely than once thought. EOS Trans., Am. Geophys. Union 77, 405–409.

Camelbeeck, T., Meghraoui, M., 1998. Geological and geophysical evidence for large palaeoearthquakes with surface faulting in the Roger Graben (Northwesten Europe). Geophys.J.Int. 132, 347–362.

Genty, D., 2008. Palaeoclimate research in Villars Cave (Dordogne, SW-France). International Journal of Speleology 37(3), 171–191.

Genty, D., Deflandre, G., 1998. Drip flow variations under a stalactite of the Père Noël cave (Belgium). Evidence of seasonal variations and air pressure constraints. Journal of Hydrology 211, 208–232.

King, G., Bilham, R., 1973. Tidal tilt measurements in Europe. Nature 243, 74–75.

Langbein, J., Burford, R., Slater, L., 1990. Variations in fault slip and strain accumulation at Parkfield, California:initial results using two color geodimeter measurements. J.Geophys.Res. 95, 2533–2552.

Melchior, P., 1983. The Tides of the Planet Earth, Pergamon Press. New York.

Sondag, F., van Ruymbeke, M., Soubiés.F., Santos, R., Somerhausen, A., Seidel, A., Boggiani, P., 2003. Monitoring present day climatic conditions in tropical caves using an environmental data acquisition system (EDAS). Journal of Hydrology 273, 103–118.

Sydenham, P., 1974. Where is experimental research on earth strain? Nature 252, 278–280.

Van Camp, M., Meus, P., Quinif, Y., Kaufmann, O., van Ruymbeke, M., Vandiepenbeeck, M., Camelbeeck, T., 2006. Karst aquifer investigation using absolute gravity. EOS Trans., Am. Geophys. Union 87, 298–299.

Van Ruymbeke, M., Beauducel, F., Somerhausen, A., 2001. The environmental data acquisition system (EDAS) developped at the Royal Observatory of Belgium. Journal of the Geodetic Society of Japan 47, 40–46.

Vandycke, S., Quinif, Y., 2001. Recent active faults in Belgian Ardenne revealed in Rochefort Karstic network (Namur province, Belgium). Netherlands Journal of Geosciences 80, 297–304.

Wenzel, H.-G., 1996. The nanogal software: Earth tide data processing package eterna 3.3. Bulletin d'Informations Marées Terrestres 124, 9425–9439.

Westerhaus, M., Zürn, W., 2001. On the use of earth tides in geodynamic research. Journal of the Geodetic Society of Japan 47 No.1, 1–9.

Yamamura, K., Sano, O., Utada, H., Takei, Y., Nakao, S., 2003. Long-term observation of in situ seismic velocity and attenuation. J.Geophys.Res. 108, doi:10.1029/2002JB002005.

Zadro, M., Braitenberg, C., 1999. Measurements and interpretations of tilt-strain gauges in seismically active areas. Earth-Science Reviews 47, 151–187.

Camelbeeck Th., van Ruymbeke M., Quinif Y., Vandycke S., de Kerkhove E., Zhu P., 2012. Obervation and interpretation of fault activity in the Rochefort cave(Belgium). Tectonophysics, 581, 48-61.

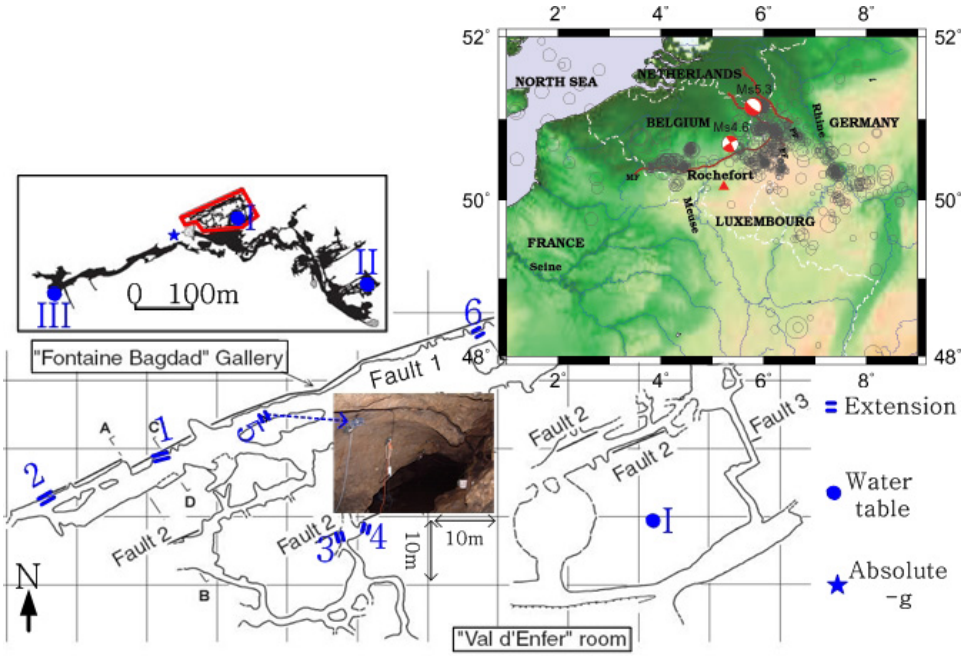

Figure 1. The sketch plot of Rochefort karstic caves, the red box marks the area at which the extensometers were installed. Three type's measurements have been conducted: extension, water table and absolute gravity. The maps on the upper right show the geological background of the site. The small photo at the center is the place where E5 was installed.

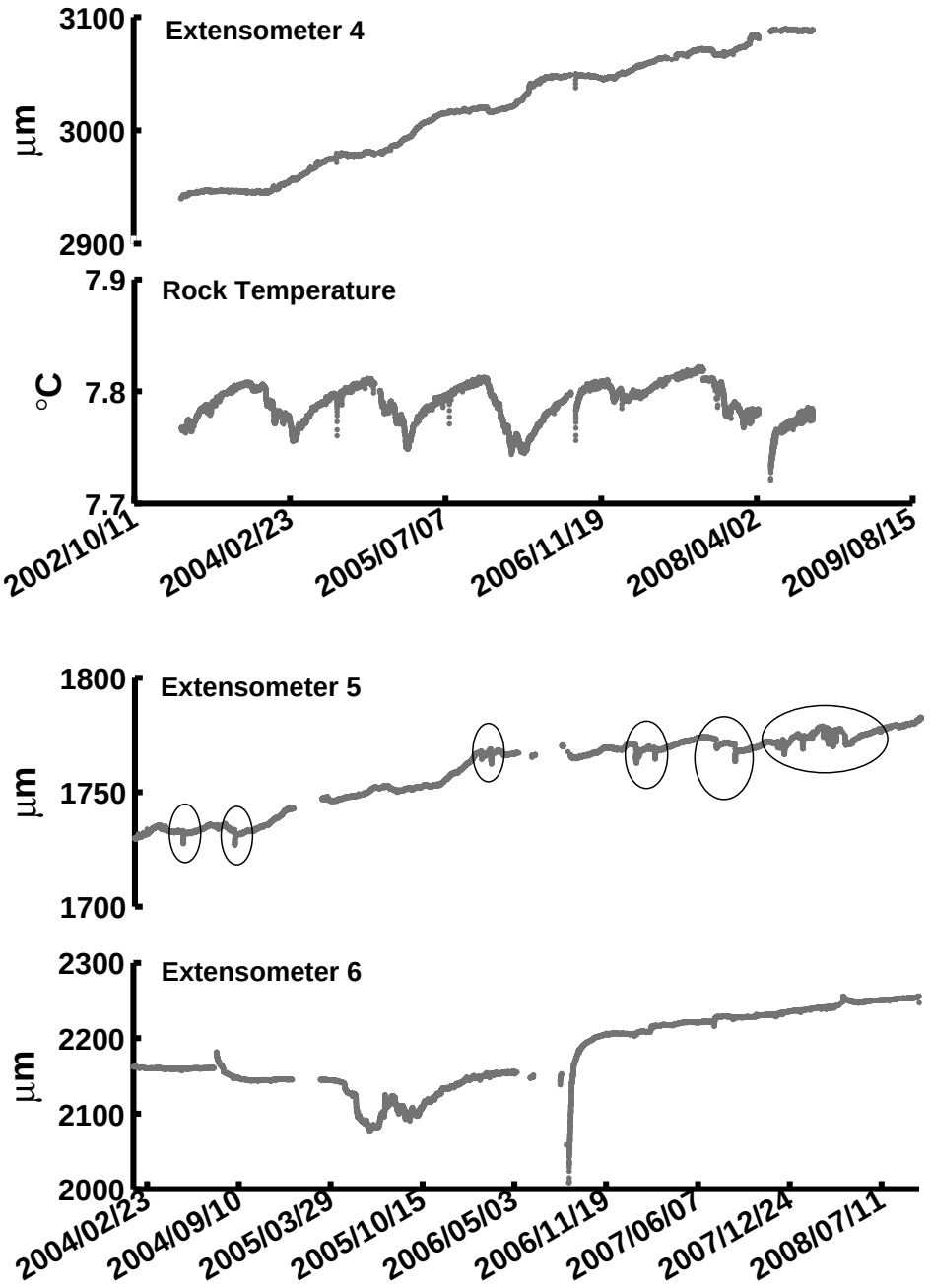

Figure 2. The original data were decimated into hour sampling rate. The annual periodical oscillations are observable from the E4 and Rock temperature. Six ellipsoidal circles mark the hydraulically induced deformation on E5. The pore pressure change during the dry season induced big gaps on E6.

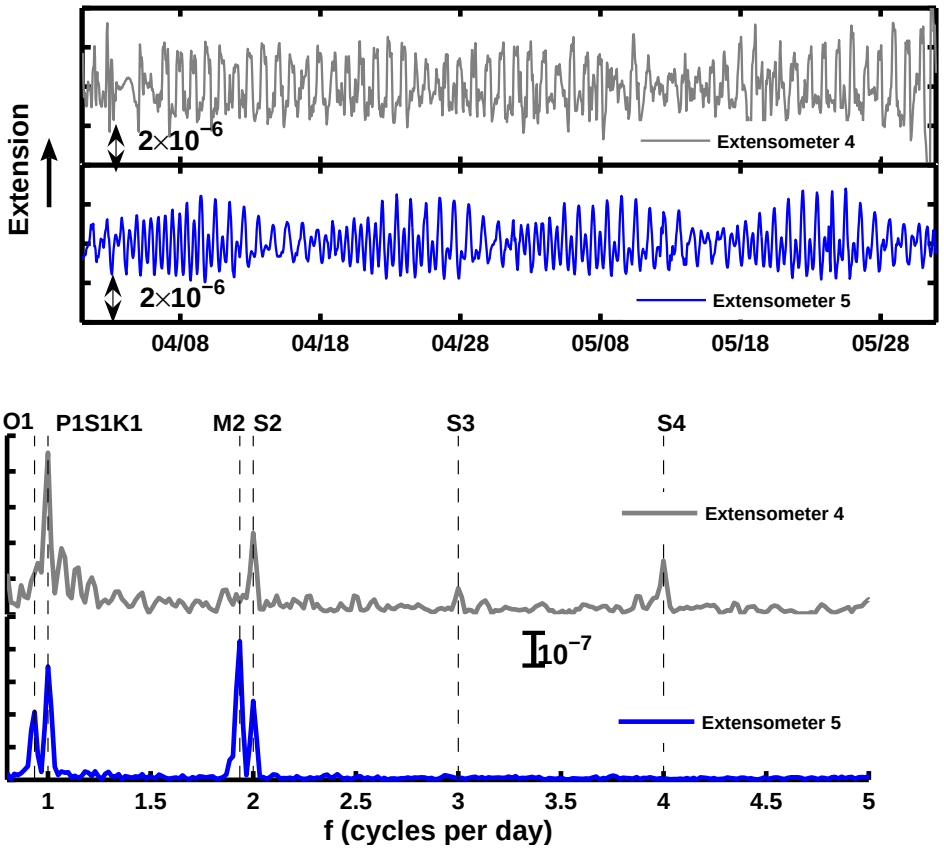

Figure 3. (Upper), The original data have been band pass filtered between 0.6 cpd and 8 cpd, the earth tides are obviously recorded by two gauges, (Lower), Amplitudes Fourier Spectrum of extensomter No. 4 and No.5.

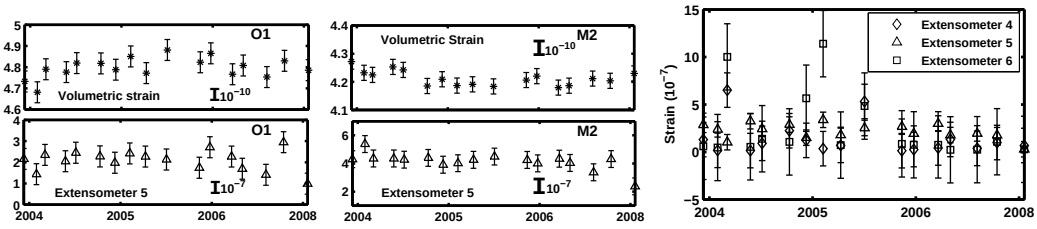

Figure 4. (a) O1 amplitudes distribution upper channel synthetic volumetric tidal strain, lower channel observed O1 tides from E5. (b) M2 amplitudes distribution upper channel synthetic volumetric tidal strain, lower channel observed M2 tides from E5. (c) S2 components separated from three sensors E4, E5 and E6.

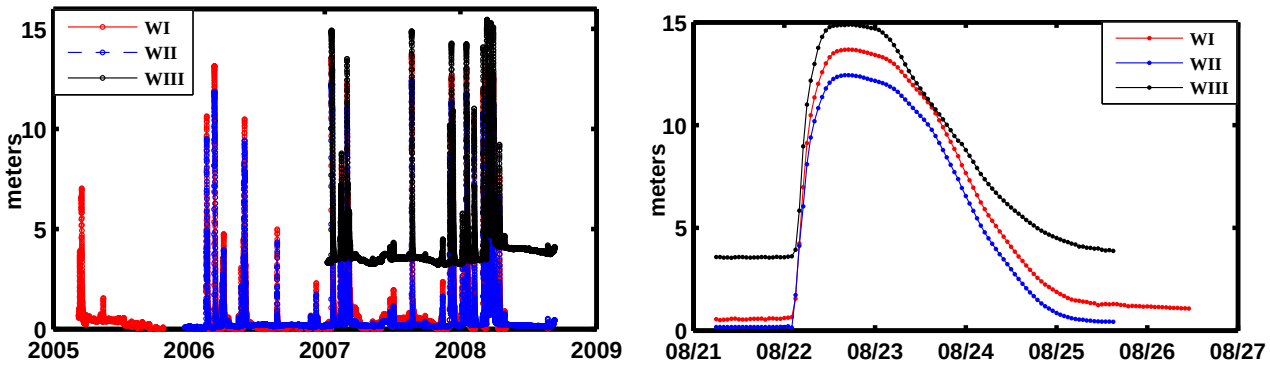

Figure 5. (Left), water table records at three locations in the karstic caves. The water level exceeded 6 meters at 16 occasions. (Right), a typical flood event recorded by three water tables.

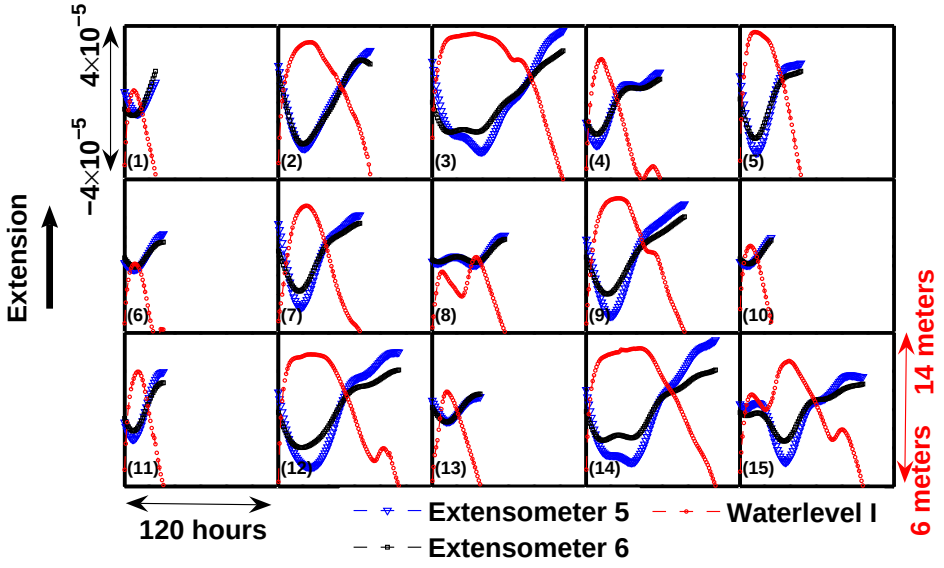

Figure 6. The water table WI, Extensometer 5, and 6 are plotted together when the water level is higher than 6 meters. The number of each box corresponds to the hydrological event listed in Table 2.

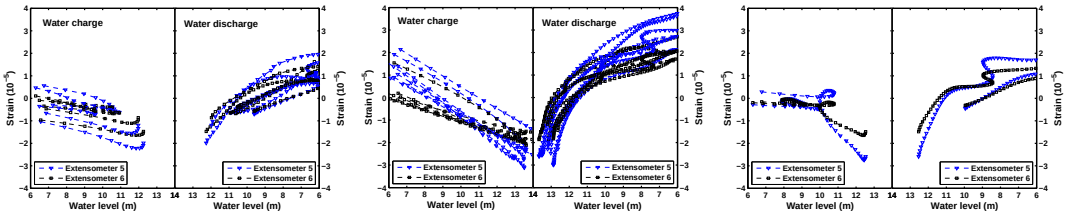

Figure 7. The strain versus water level. (a) The first type, the duration of water level higher than 6 meters is shorter than 10 hours. (b) The second type, the duration of water level higher than 6 meters is longer than 10 hours. (c) The third type, more than one times the water level rose higher than 6 meters.

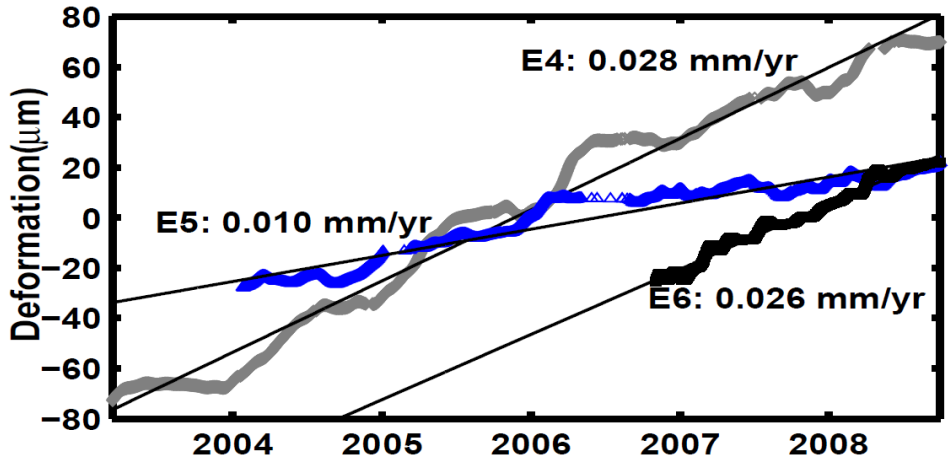

Figure 8. The long term trend of E4, E5 and E6 is fitted by a linear function with 95% confidential level.

Table 1. Tidal analysis result of E5 records between Apr.01 and Sept.30 2005. Synthetic volumetric strain is compared with the observations.

Wave	E5(10^{-7})	Syn(10^{-9})	Ratio	E5(ϕ)	Syn(ϕ)	Diff.
O1	2.219	5.006	44.3	138.311	125.186	13.125
M2	3.798	4.593	82.7	134.988	138.229	-3.241
S2	1.859	1.623	114.5	12.112	8.122	3.990

Table 2. Hydrological events were separated into three groups, the maximum strain changes corresponding to the highest water is measured from each event.

NO.	Date	Dur(hrs)	WI(m)	E5(10^{-5})	E6(10^{-5})
1	2006/02/17 00:00	25	10.6	-1.18	-0.33
4	2007/03/01 11:00	5	12.3	-1.20	-0.68
6	2007/12/03 03:00	31	9.6	-0.09	-0.13
10	2008/02/06 09:00	25	10.5	-0.04	-0.09
11	2008/03/01 09:00	9	11.9	-0.90	-0.65
13	2008/03/16 20:00	38	10.9	-1.11	-0.76
2	2006/03/09 06:00	72	13.1	-4.35	-3.69
3	2007/01/18 06:00	102	13.6	-4.75	-1.56
5	2007/08/22 05:00	48	13.7	-4.05	-2.05
7	2007/12/06 23:00	64	12.6	-4.42	-2.09
9	2008/01/16 02:00	77	13.0	-4.04	-1.92
12	2008/03/11 08:00	94	12.9	-3.93	-1.84
14	2008/03/21 06:00	101	13.2	-3.84	-1.49
8	2007/12/10 05:00	57	9.9	-0.19	-0.13
15	2008/03/31 22:00	96	12.5	-3.07	-1.49